2015 IEEE International Conference on Robotics and Automation (ICRA)
Washington State Convention Center
Seattle, Washington, May 26-30, 2015

Unified Passivity-Based Cartesian Force/Impedance Control for Rigid and Flexible Joint Robots via Task-Energy Tanks

Christopher Schindlbeck and Sami Haddadin

Abstract— **In this paper we propose a novel hybrid Cartesian force/impedance controller that is equipped with energy tanks to preserve passivity. Our approach overcomes the problems of (hybrid) force control, impedance control, and set-point based indirect force control. It allows accurate force tracking, full compliant impedance behavior, and safe contact resemblance simultaneously by introducing a controller shaping function that robustly handles unexpected contact loss and avoids chattering behavior that switching based approaches suffer from. Furthermore, we propose a constructive way of initiating the energy tanks via the concept of task energy. This represents an estimate of the energy consumption of a given force control task prior to execution. The controller can be applied to both rigid body and flexible joint dynamics. To show the validity of our approach, several simulations and experiments with the KUKA/DLR LWR-III are carried out.**

I. INTRODUCTION AND STATE-OF-THE-ART

Nowadays, robotic systems outperform humans in terms of repetitive speed and precision tasks. In terms of sensitive force and compliance control humans still show superior performance. However, at the same time an increasing set of tasks in robotic manipulation, and in particular also in real-world applications, deals now always with sensitive object handling and assembly. This requires an intricate coordination of contact force and motion generation for which sophisticated control algorithms were developed over the last decades. In this context, impedance control [1] has become one of the most popular concepts, which aims for mimicking human behavior by imposing mass-spring-damper-like disturbance response via active control on the robot. In general, compliance in robotic systems, either achieved via active control or by deliberately introducing compliant mechanical elements into the drive train[1], has become very popular due to their ability to cope with process uncertainty and exert only well defined force ranges on their environment or the objects they manipulate. In this paper we focus on extending the concepts from active compliance control.

Active interaction control can be subdivided into direct and indirect force control [3]. Recently, indirect force controllers using set-point generation [4], [5] were introduced. A constraint-based access to control force, position, and impedance in different subspaces was proposed in [6]. Despite the significant progress that was made in the domain of force control, some basic problems remained. For example, an impedance controller executes desired forces either via a pure feed-forward force or through a virtual displacement. Therefore, these controllers do not take into account sensed external forces. Hence, in order to accurately apply desired forces, the surface geometry and the contact properties such as stiffness need to be known a-priori. This contradicts the core idea of impedance control to work effectively in unmodeled environments. Furthermore, this paradigm has the drawback that when applying a larger force with such a feed-forward approach and then unexpectedly loosing contact with the environment, this may result in an undesired and possibly very unsafe motion of the robot towards the (distant) set-point. This happens due to an instantaneous energy release of the potential energy stored in the preloaded spring into kinetic energy.

Fig. 1. Polishing the front apron of a car. A normal force shall be applied to the unknown surface, while perpendicular circular motions cover the area that has to be polished.

The direct force control paradigm provides the basics to accurately exchange contact forces and thus directly manipulate objects or apply forces on surfaces. This capability is also a core necessity in industrial applications, since the rather imprecise impedance control based force regulation, or let alone position control, do not suffice due to modeling and/or planning errors, resulting in possibly large process uncertainties. This problem has led to approaches such as hybrid position/force control [7], which idea is to partition the task space into complementary force and motion subspaces such that force and motion control is only applied in

The authors are with the Institute of Automatic Control, Faculty of Electrical Engineering and Computer Science, Leibniz Universität Hannover, 30167 Hannover, Germany {schindlbeck,haddadin}@irt.uni-hannover.de

[1]However, it is usually not possible to display arbitrary Cartesian compliance with uncoupled elastic joints only [2], making it necessary to combine passive compliance with active control to solve the issue.

978-1-4799-6923-4/15/$31.00 ©2015 IEEE

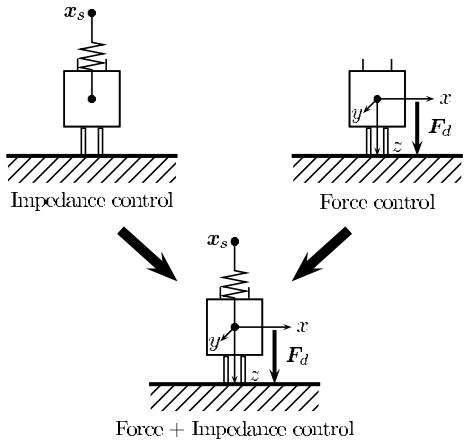

Fig. 2. Conceptual schematic of the proposed controller (dampers are not shown for simplicity). Top left: purely impedance controlled robot. Top right: force controlled robot. Bottom: Combining force and impedance control.

its respective subspace.

However, a major drawback of (hybrid) force control methods is that they show very low robustness with respect to contact loss. Furthermore, the contact properties of the environment need to be modeled very accurately for good performance, which is hardly ever the case. Furthermore, in order to determine the stability properties of force controllers, the environment is typically modeled as a simple spring-damper system. An overview of different classical force control algorithms, including remarks on their respective stability properties can be found in [8]. A very general critique regarding hybrid force/motion control was also formulated in [9] that was based on the problem of coordinate choice and the respective choice of metric.

In this paper, we strive for a robust passivity-based approach by combining force tracking with impedance control (see Figure 2) based on the concept of energy tanks [10], [11]. Our approach guarantees stability for arbitrary passive environments and has no need to apply set-point variations, which show rather inaccurate behavior for general environments. Our solution allows for robust, compliant, and stable manipulations without the need to chose between force or impedance control, but rather unify the best of all. Furthermore, we present a solution that is able to get rid of the inherent drawback of force and set-point based indirect force control: the low robustness with respect to contact loss and the according possibility of unsafe abrupt robot motions. In summary, the contributions of this paper are as follows.

1) Simultaneous passivity-based impedance control and wrench regulation/tracking
2) Stability proof for arbitrary passive environments instead of model-based environments
3) Suitable for rigid and flexible joint robot models
4) Task-based energy tank design and initialization
5) Contact-non-contact stabilization

Subsequently, the considered robot dynamics and thereafter the proposed controller are outlined.

II. MODELING

A. Rigid Robot Dynamics

The well-known rigid body dynamics of a robot with n joints can be written as

$$M(\boldsymbol{q})\ddot{\boldsymbol{q}} + C(\boldsymbol{q},\dot{\boldsymbol{q}})\dot{\boldsymbol{q}} + \boldsymbol{g}(\boldsymbol{q}) = \boldsymbol{\tau}_m + \boldsymbol{\tau}_{ext}, \tag{1}$$

where $\boldsymbol{q} \in \mathbb{R}^n$ is the link position. The mass matrix is denoted by $M(\boldsymbol{q}) \in \mathbb{R}^{n\times n}$, the Coriolis and centrifugal vector by $C(\boldsymbol{q},\dot{\boldsymbol{q}})\dot{\boldsymbol{q}} \in \mathbb{R}^n$, and the gravity vector by $\boldsymbol{g}(\boldsymbol{q}) \in \mathbb{R}^n$. The control input of the system is the motor torque $\boldsymbol{\tau}_m \in \mathbb{R}^n$, while $\boldsymbol{\tau}_{ext} \in \mathbb{R}^n$ comprises all externally applied torques[2]. External forces are denoted via the Cartesian space wrench $\boldsymbol{F}_{ext} := (\boldsymbol{f}_{ext}^T, \boldsymbol{m}_{ext}^T)^T \in \mathbb{R}^6$, comprising a force/torque vector. This wrench can be mapped via the contact Jacobian $J^T(\boldsymbol{q})$ to joint space external torques $\boldsymbol{\tau}_{ext} = J^T(\boldsymbol{q})\boldsymbol{F}_{ext}$.

B. Flexible Joint Dynamics

For lightweight or SEA-type systems, (1) is not sufficiently accurate to describe the inherent dynamics due to the presence of flexible transmission. Therefore, the (reduced) flexible joint model will be considered for such structures, which is described by [12]

$$M(\boldsymbol{q})\ddot{\boldsymbol{q}} + C(\boldsymbol{q},\dot{\boldsymbol{q}})\dot{\boldsymbol{q}} + \boldsymbol{g}(\boldsymbol{q}) = \boldsymbol{\tau}_J + \boldsymbol{\tau}_{ext} \tag{2}$$

$$B\ddot{\boldsymbol{\theta}} + \boldsymbol{\tau}_J = \boldsymbol{\tau}_m \tag{3}$$

$$\boldsymbol{\tau}_J = K(\boldsymbol{\theta} - \boldsymbol{q}), \tag{4}$$

with $\boldsymbol{\theta} \in \mathbb{R}^n$ being the motor position. Equations (2) and (3) constitute the link- and motor-side dynamics, respectively. Equation (4) couples (2) and (3) via the elastic joint torque $\boldsymbol{\tau}_J \in \mathbb{R}^n$, which is considered to have linear spring-like characteristics. Damping in the joint torque may be also considered, but the extension is rather trivial and will therefore not be considered here. The matrices $K \in \mathbb{R}^{n\times n}$ and $B \in \mathbb{R}^{n\times n}$ are both constant diagonal positive definite matrices, expressing the lumped joint stiffness and motor inertia, respectively. Neither motor nor link side friction are considered for sake of clarity.

III. CONTROLLER DESIGN AND ANALYSIS

A. Preliminaries: Flexible Joint Cartesian Impedance Control

Impedance control for the flexible joint case can be realized such that passivity is preserved. This is achieved by making the position feedback to be a function of $\boldsymbol{\theta}$ only instead of both $\boldsymbol{\theta}$ and $\boldsymbol{q}$. For this, $\boldsymbol{q}$ is replaced with its static equivalent $\bar{\boldsymbol{q}}(\boldsymbol{\theta}) = \boldsymbol{\zeta}^{-1}(\boldsymbol{\theta})$, which is numerically obtained by a contraction mapping with the implicit function $\boldsymbol{\zeta}(\boldsymbol{q}_e) = \boldsymbol{q}_e + K^{-1}\boldsymbol{g}(\boldsymbol{q}_e)$, where $\boldsymbol{q}_e$ is the joint position at the equilibrium point. Under mild assumptions $\bar{\boldsymbol{q}}(\boldsymbol{\theta})$ can be used as an estimate for $\boldsymbol{q}$. For more details on the implicit function $\boldsymbol{\zeta}$ as well as the underlying theory, please see [13]. The

[2]Friction is not explicitly considered for simplicity.

passivity-based impedance law for the flexible joint robot can then be formulated as

$$\boldsymbol{\tau}_{mi} = -J^T(\bar{\boldsymbol{q}})(K_x\tilde{\boldsymbol{x}}(\bar{\boldsymbol{q}}(\boldsymbol{\theta})) + D_x\dot{\boldsymbol{x}}) \tag{5}$$

$$\tilde{\boldsymbol{x}}(\boldsymbol{\theta}) = \tilde{\boldsymbol{x}}(\bar{\boldsymbol{q}}(\boldsymbol{\theta})) = \boldsymbol{f}(\bar{\boldsymbol{q}}(\boldsymbol{\theta})) - \boldsymbol{x}_s = \boldsymbol{x}(\boldsymbol{\theta}) - \boldsymbol{x}_s \tag{6}$$

$$\dot{\boldsymbol{x}}(\boldsymbol{\theta}) = J(\bar{\boldsymbol{q}})\dot{\boldsymbol{\theta}}, \tag{7}$$

where $\boldsymbol{\tau}_m = \boldsymbol{\tau}_{mi}$ in (3). For simplicity, we assume $\dot{\boldsymbol{x}}(\boldsymbol{\theta}) = J(\bar{\boldsymbol{q}})\dot{\boldsymbol{\theta}} \approx J(\boldsymbol{q})\dot{\boldsymbol{q}} = \dot{\boldsymbol{x}}$. The mapping $\boldsymbol{f} : \mathbb{R}^n \to \mathbb{R}^6$ encodes the forward kinematics while $\boldsymbol{x}_s \in \mathbb{R}^6$ denotes the (constant) impedance set-point. (7) relates joint space velocities to Cartesian space velocities by the task Jacobian J. The matrices $K_x \in \mathbb{R}^{6\times6}$ and $D_x \in \mathbb{R}^{6\times6}$ are positive definite matrices for stiffness and damping, respectively. D_x can be chosen manually (constant, often diagonal) or obtained by appropriate damping design [14] (time-varying, non-diagonal) such that e.g. critical damping is achieved even for varying configuration. Nevertheless, positive definiteness is ensured in both cases. Additionally, joint torque feedback can be used to scale the motor inertia and obtain an auxiliary control input [15]. This is a special case which can be realized when the robot is equipped joint torque sensing[3].

B. Basic Controller Design: Force Tracking

In our controller design we start from the following Cartesian force tracking controller

$$\begin{aligned}\boldsymbol{\tau}_{mf} = J^T(\bar{\boldsymbol{q}})\Big[&K_p(\boldsymbol{F}_{ext}(t) - \boldsymbol{F}_d(t)) \\ &+ K_d(\dot{\boldsymbol{F}}_{ext}(t) - \dot{\boldsymbol{F}}_d(t)) \\ &+ K_i\int_0^t (\boldsymbol{F}_{ext}(\sigma) - \boldsymbol{F}_d)\,d\sigma\Big],\end{aligned} \tag{8}$$

where $K_p \in \mathbb{R}^{6\times6}$, $K_d \in \mathbb{R}^{6\times6}$ and $K_i \in \mathbb{R}^{6\times6}$ are diagonal positive definite matrices for proportional, derivative and integral control part, respectively. The desired wrench $\boldsymbol{F}_d(t) := (\boldsymbol{f}_d^T(t), \boldsymbol{m}_d^T(t))^T \in \mathbb{R}^6$ is specified by the user (or generated by a planner) in order to apply a desired force/torque on the environment. For convenience, we define $\boldsymbol{h}_i(\boldsymbol{F}_{ext}, t) := \int_0^t (\boldsymbol{F}_d(\sigma) - \boldsymbol{F}_{ext}(\sigma))d\sigma$. $\boldsymbol{F}_{ext}$ can be obtained e.g. via a force/torque sensor or so-called sensor-less methods [16]. However, the estimation dynamics would have to be considered then as well. Applying the force controller $\boldsymbol{\tau}_m = \boldsymbol{\tau}_{mf}$ to a rigid robot would lead to insertion of the motor torque (8) into (1) and to insertion into (3) for a flexible joint robot. Subsequently, we prove the stability of the controller for the flexible joint case[4].

C. Stability Analysis: Part I

In order to prove the stability we first decompose the entire system into three parts (see Figure 3), namely

I Environment
II Rigid body dynamics
III Motor dynamics + Force/Impedance Controller

[3]However, this would not change any results in this paper and is thus omitted.

[4]The rigid robot case will be omitted since is it a special case and stability can be proven in a similar rather straightforward fashion.

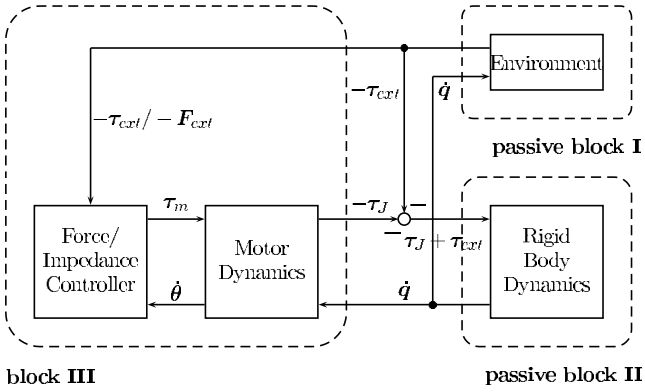

Fig. 3. Parallel and feedback interconnection of blocks with their respective input and output ports.

It is well-known that it is sufficient to prove that each part is passive w.r.t. their input-output ports if the blocks are connected in parallel or in feedback [17]. Since the rigid body dynamics (2) are passive w.r.t. the input-output pair $[\boldsymbol{\tau}_J + \boldsymbol{\tau}_{ext}, \dot{\boldsymbol{q}}]$ and we assume the environment to be passive w.r.t. $[\dot{\boldsymbol{q}}, -\boldsymbol{\tau}_{ext}]$. This leaves only to prove that block III is passive w.r.t. $[\dot{\boldsymbol{q}}, -\boldsymbol{\tau}_J]$ for proving the entire system's stability. This block has shown to be passive without the force controller in [13] and therefore also without the feedback of $-\boldsymbol{\tau}_{ext}/-\boldsymbol{F}_{ext}$. Adding (5) and (8) combines the impedance and force controller for the flexible joint case via $\boldsymbol{\tau}_m = \boldsymbol{\tau}_{mi} + \boldsymbol{\tau}_{mf}$ and leads to the overall controller

$$\begin{aligned}\boldsymbol{\tau}_m = -J^T(\boldsymbol{q})\Big[&K_p(\boldsymbol{F}_d(t) - \boldsymbol{F}_{ext}(t)) + K_d(\dot{\boldsymbol{F}}_d(t) \\ &- \dot{\boldsymbol{F}}_{ext}(t)) + K_i\boldsymbol{h}_i(\boldsymbol{F}_{ext}, t) + K_x\tilde{\boldsymbol{x}}(\boldsymbol{\theta}) + D_x\dot{\boldsymbol{x}}\Big].\end{aligned} \tag{9}$$

As delineated in [13] it is generally sufficient to analyze the passivity w.r.t. $[\dot{\boldsymbol{\theta}}, -\boldsymbol{\tau}_J]$ instead of $[\dot{\boldsymbol{q}}, -\boldsymbol{\tau}_J]$ for a flexible joint robot due to the relation

$$\begin{aligned}-\dot{\boldsymbol{q}}^T\boldsymbol{\tau}_J =& \frac{d}{dt}\left(\frac{1}{2}(\boldsymbol{\theta} - \boldsymbol{q})^T K(\boldsymbol{\theta} - \boldsymbol{q})\right) - \dot{\boldsymbol{\theta}}^T\boldsymbol{\tau}_J \\ =& \dot{S}_\theta - \dot{\boldsymbol{\theta}}^T\boldsymbol{\tau}_J,\end{aligned} \tag{10}$$

where $S_\theta := \frac{1}{2}(\boldsymbol{\theta}-\boldsymbol{q})^T K(\boldsymbol{\theta}-\boldsymbol{q})$ is a positive definite storage function. We can now conclude[5] from (3) and (9)

$$\begin{aligned}-\dot{\boldsymbol{\theta}}^T\boldsymbol{\tau}_J =& \dot{\boldsymbol{\theta}}^T B\ddot{\boldsymbol{\theta}} - \dot{\boldsymbol{\theta}}^T\boldsymbol{\tau}_m \\ =& \dot{\boldsymbol{\theta}}^T B\ddot{\boldsymbol{\theta}} + \underbrace{\dot{\boldsymbol{\theta}}^T J^T}_{\approx\dot{\boldsymbol{x}}^T}\Big[K_p(\boldsymbol{F}_d - \boldsymbol{F}_{ext}) \\ &+ K_d(\dot{\boldsymbol{F}}_d - \dot{\boldsymbol{F}}_{ext}) + K_i\boldsymbol{h}_i + K_x\tilde{\boldsymbol{x}} + D_x\dot{\boldsymbol{x}}\Big] \\ =& \dot{S}_M + \dot{S}_I + \dot{\boldsymbol{x}}^T D_x\dot{\boldsymbol{x}} + \dot{\boldsymbol{x}}^T K_p(\boldsymbol{F}_d - \boldsymbol{F}_{ext}) \\ &+ \dot{\boldsymbol{x}}^T K_d(\dot{\boldsymbol{F}}_d - \dot{\boldsymbol{F}}_{ext}) + \dot{\boldsymbol{x}}^T K_i\boldsymbol{h}_i,\end{aligned} \tag{11}$$

with $S_M(\boldsymbol{\theta}) := \frac{1}{2}\dot{\boldsymbol{\theta}}^T B\dot{\boldsymbol{\theta}}$ and $S_I(\tilde{\boldsymbol{x}}) := \frac{1}{2}\tilde{\boldsymbol{x}}^T K_x\tilde{\boldsymbol{x}}$. While $S_\theta + S_I + S_M$ has proven to be positive definite, it is

[5]Subsequently, we drop dependencies for readability.

unfortunately not possible to derive the sign of any of the last three terms in (11). Thus, the passivity of block III is potentially violated.

D. Controller Design: Energy Tank Design

In order to solve the aforementioned problem and preserve the passivity at all times, we use the concept of energy tanks to modify the controller and add a tank element to the former block III (from now on: block IV, see Figure 4) such that passivity is preserved. Up to now, the concept of energy tanks has been mainly used in teleoperation [18], [19], [20] and was only recently applied to impedance control in terms of variable stiffness [21], [22]. Subsequent proof follows similar lines of thought.

First, we introduce the virtual tank, which state is denoted as x_t and its output as $y_t = x_t$. The associated tank energy is $T = \frac{1}{2}x_t^2$, while its dynamics is defined as[6]

$$\dot{x}_t = \frac{\beta}{x_t}(\dot{\boldsymbol{x}}^T D_x \dot{\boldsymbol{x}} + \gamma \dot{\boldsymbol{x}}^T K_d(\dot{\boldsymbol{F}}_d - \dot{\boldsymbol{F}}_{ext})) + u_t, \tag{12}$$

where β is defined as

$$\beta = \begin{cases} 1 & \text{if } T \leq T^u \\ 0 & \text{else.} \end{cases} \tag{13}$$

Its purpose is to avoid further tank loading via dissipative terms if a certain upper limit storage T^u is reached. The control input of the tank is chosen to be $u_t = -\boldsymbol{\omega}^T \dot{\boldsymbol{x}}$ with

$$\begin{aligned} \boldsymbol{\omega}(\boldsymbol{F}_{ext}, t) = &\frac{\alpha}{x_t}\Big(K_p(\boldsymbol{F}_{ext} - \boldsymbol{F}_d) \\ &+ (1-\gamma)K_d(\dot{\boldsymbol{F}}_d - \dot{\boldsymbol{F}}_{ext}) - K_i \boldsymbol{h}_i(\boldsymbol{F}_{ext}, t)\Big), \end{aligned} \tag{14}$$

where α is defined as

$$\alpha = \begin{cases} 1 & \text{if } T \geq T_l \\ 0 & \text{else.} \end{cases} \tag{15}$$

α is responsible for detaching the energy tank from the force/impedance controller if the lower limit of the energy tank T_l is reached. Therefore, in order to avoid the singularity in (14), the lower limit needs to be greater than zero, i.e. $T_l > 0$. γ is defined as

$$\gamma = \begin{cases} 1 & \text{if } \dot{\boldsymbol{x}}^T K_d(\dot{\boldsymbol{F}}_d - \dot{\boldsymbol{F}}_{ext}) \geq 0 \\ 0 & \text{else.} \end{cases} \tag{16}$$

Its meaning will become evident in Section III-E when proving the stability of the system. Based on $\boldsymbol{\omega}(\boldsymbol{F}_{ext}, t)$ from (14) we can rewrite the motor dynamics (3) as

$$\begin{aligned} -\boldsymbol{\tau}_J = &B\ddot{\boldsymbol{\theta}} + J^T(\boldsymbol{q})\Big[K_x\tilde{\boldsymbol{x}} + D_x\dot{\boldsymbol{x}} + \gamma K_d(\dot{\boldsymbol{F}}_d - \dot{\boldsymbol{F}}_{ext}) \\ &- \boldsymbol{\omega} x_t\Big] =: B\ddot{\boldsymbol{\theta}} - \boldsymbol{\tau}'_m, \end{aligned} \tag{17}$$

[6]Note that for sake of clarity we do not consider the nullspace of a redundant robot.

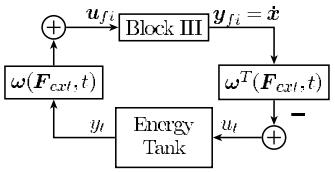

Fig. 5. Power-preserving feedback interconnection of force/impedance controller + motor dynamics and the energy tank.

where $\boldsymbol{\tau}'_m$ is our proposed control law for the force/impedance controller including energy tank. Subsequently, we define the input of the force/impedance controller to be $\boldsymbol{u}_{fi} = \boldsymbol{\omega} x_t$ and the output to be $\boldsymbol{y}_{fi} = \dot{\boldsymbol{x}}$. The energy tank is connected to the force/impedance controller via a power-preserving Dirac structure [11]

$$\begin{pmatrix} \boldsymbol{u}_{fi} \\ u_t \end{pmatrix} = \begin{bmatrix} 0_{6\times 6} & \boldsymbol{\omega} \\ -\boldsymbol{\omega}^T & 0 \end{bmatrix} \begin{pmatrix} \boldsymbol{y}_{fi} \\ y_t \end{pmatrix}, \tag{18}$$

which can be interpreted as a feedback structure, see Figure 5.

E. Stability Analysis: Part II

Due to the lossless connection (18) we can write the storage function of block IV as

$$\begin{aligned} S(\dot{\boldsymbol{\theta}}, \tilde{\boldsymbol{x}}, x_t) &= S_M(\boldsymbol{\theta}) + S_I(\tilde{\boldsymbol{x}}) + T(x_t) \\ &= \frac{1}{2}\dot{\boldsymbol{\theta}}^T B \dot{\boldsymbol{\theta}} + \frac{1}{2}\tilde{\boldsymbol{x}}^T K_x \tilde{\boldsymbol{x}} + \frac{1}{2}x_t^2. \end{aligned} \tag{19}$$

Evaluating the timely evolution along the motor dynamics (17) and tank dynamics (12) leads to

$$\begin{aligned} \dot{S}(\dot{\boldsymbol{\theta}}, \tilde{\boldsymbol{x}}, x_t) = &-\dot{\boldsymbol{\theta}}^T \boldsymbol{\tau}_J - \dot{\boldsymbol{x}}^T D_x \dot{\boldsymbol{x}} - \dot{\boldsymbol{x}}^T \gamma K_d(\dot{\boldsymbol{F}}_d - \dot{\boldsymbol{F}}_{ext}) \\ &+ \dot{\boldsymbol{x}}^T \boldsymbol{\omega} x_t \\ &+ \beta\left(\dot{\boldsymbol{x}}^T D_x \dot{\boldsymbol{x}} + \dot{\boldsymbol{x}}^T \gamma K_d(\dot{\boldsymbol{F}}_d - \dot{\boldsymbol{F}}_{ext})\right) \\ &- x_t \boldsymbol{\omega}^T \dot{\boldsymbol{x}} \\ = &-\dot{\boldsymbol{\theta}}^T \boldsymbol{\tau}_J - \dot{\boldsymbol{x}}^T D_x \dot{\boldsymbol{x}} - \gamma \dot{\boldsymbol{x}}^T K_d(\dot{\boldsymbol{F}}_d - \dot{\boldsymbol{F}}_{ext}) \\ &+ \beta\left(\dot{\boldsymbol{x}}^T D_x \dot{\boldsymbol{x}} + \gamma \dot{\boldsymbol{x}}^T K_d(\dot{\boldsymbol{F}}_d - \dot{\boldsymbol{F}}_{ext})\right). \end{aligned} \tag{20}$$

Since $S(\dot{\boldsymbol{\theta}}, \tilde{\boldsymbol{x}}, x_t) \geq 0$ and obviously $\dot{S}(\dot{\boldsymbol{\theta}}, \tilde{\boldsymbol{x}}, x_t) = \dot{S}(\dot{\boldsymbol{\theta}}, \tilde{\boldsymbol{x}}) \leq -\dot{\boldsymbol{\theta}}^T \boldsymbol{\tau}_J$ due to (13) and (16), block IV is passive. Basically, the energy tank dynamically cancels out the non-passive terms which arise during contact such that block IV is passive w.r.t. $[\dot{\boldsymbol{\theta}}, -\boldsymbol{\tau}_J]$ and therefore $[\dot{\boldsymbol{q}}, -\boldsymbol{\tau}_J]$. Hence, the overall system is shown to be stable.

F. Contact-loss Stabilization

Although stability is now guaranteed in all cases, this does not mean that the robot could not execute unsafe motions. Unexpected loss of contact with the surface would e.g. mean that the robot still tries to regulate a force and it would do this until the tank is drained. Depending on the remaining energy in the tank, this may lead to fast and large unwanted motions. In order to prevent this problem, one could intuitively suggest to deactivate the controller when no contact

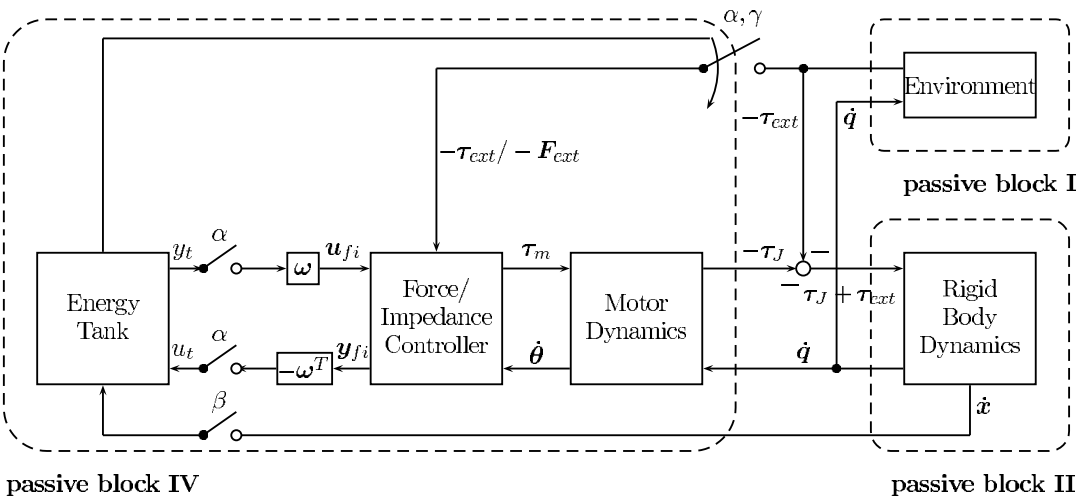

Fig. 4. Parallel and feedback interconnection of blocks with their respective input and output ports with an additional energy tank. Interpretation: By detaching the controller if passivity is possibly violated ($\alpha = 0$, $\gamma = 0$) the feedback of external forces is canceled.

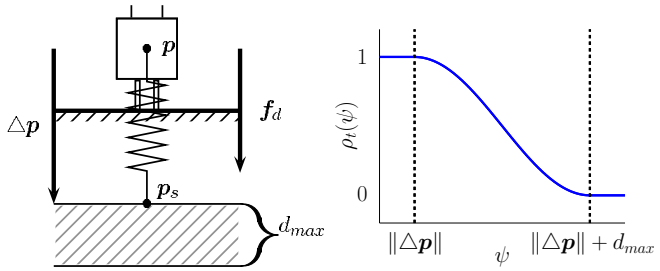

Fig. 6. Left: Impedance controlled robot with translational robustness region d_{max}. Right: Controller shaping function for the translational case.

is detected. However, this would lead to undesired switching behavior due to sensor noise, a typical and basically unsolved problem in force control. Here, we propose a more robust and provably stable way by introducing a controller shaping function $\boldsymbol{\rho}(\psi)$, where ψ is a shifted variable w.r.t. $\|\triangle \boldsymbol{p}\|$ in the translational case or $\triangle\varphi$ in the rotational case. This function is incorporated into the overall controller as follows:

$$\boldsymbol{\rho}(\psi) = (\rho_t(\psi), \rho_t(\psi), \rho_t(\psi), \rho_r(\psi), \rho_r(\psi), \rho_r(\psi))^T$$

is composed of a translational part $\rho_t(\psi)$, which is defined as

$$\rho_t(\psi) = \begin{cases} 1 & \text{if } \boldsymbol{f}_d^T \triangle \boldsymbol{p} \geq 0 \\ \frac{1}{2}\left[1 + \cos\left(\frac{\psi - \|\triangle \boldsymbol{p}\|}{d_{max}}\pi\right)\right] & \text{if } \boldsymbol{f}_d^T \triangle \boldsymbol{p} < 0 \\ & \wedge \psi \in [\|\triangle \boldsymbol{p}\|, \\ & \quad \|\triangle \boldsymbol{p}\| + d_{max}] \\ 0 & \text{else} \end{cases} \tag{21}$$

and a rotational part $\rho_r(\psi)$ defined as

$$\rho_r(\psi) = \begin{cases} 1 & \text{if } \boldsymbol{m}_d^T \triangle k_0 \triangle \boldsymbol{k}_v \geq 0 \\ \frac{1}{2}\left[1 + \cos\left(\frac{\psi - \triangle\varphi}{\varphi_{max}}\pi\right)\right] & \text{if } \boldsymbol{m}_d^T \triangle k_0 \triangle \boldsymbol{k}_v < 0 \\ & \wedge \psi \in [\triangle\varphi, \\ & \quad \triangle\varphi + \varphi_{max}] \\ 0 & \text{else.} \end{cases} \tag{22}$$

We define $\boldsymbol{x} := (\boldsymbol{p}^T, \boldsymbol{\varphi}^T)^T$ to be comprised of a translational part $\boldsymbol{p}$ and a chosen rotational representation, e.g. Euler angles $\boldsymbol{\varphi}$. In (21), $\triangle \boldsymbol{p} = \boldsymbol{p}_s - \boldsymbol{p}$ denotes the vector that points from the end-effector position to the set-point and $\boldsymbol{F}_d := (\boldsymbol{f}_d^T, \boldsymbol{m}_d^T)^T$ is the desired wrench (see Figure 6). If $\triangle \boldsymbol{p}$ and $\boldsymbol{f}_d$ enclose an angle greater than 90° the controller should be deactivated. In order to ensure a smooth transition instead of a chattering behavior $\rho_t(\psi)$ interpolates in a user-defined region of width d_{max}. For the rotational part $\rho_r(\psi)$ we choose the singularity-free quaternion representation. The unit quaternion $\boldsymbol{k} = (k_0, \boldsymbol{k}_v)$ denotes the current orientation and the quaternion $\boldsymbol{k}_s = (k_{0,s}, \boldsymbol{k}_{v,s})$ the desired orientation. The rotation error is then defined as $\triangle \boldsymbol{k} := \boldsymbol{k}^{-1}\boldsymbol{k}_s$ and $\triangle\varphi := 2\arccos(\triangle k_0)$. The user-defined rotational robustness region can then be specified as an angle φ_{max}, which relates to the scalar component of the quaternion by $\varphi_{max} = 2\arccos(k_{0,max})$.

From a stability point of view, the controller shaping function can be interpreted as shaping $\boldsymbol{\omega}$ since it only scales the force controller part of the combined force/impedance controller. Therefore, (14) can simply be redefined as

$$\boldsymbol{\omega}_\rho(\boldsymbol{F}_{ext}, t) := \begin{pmatrix} \rho_t(\psi)\mathbf{1}_{3\times1} \\ \rho_r(\psi)\mathbf{1}_{3\times1} \end{pmatrix} \boldsymbol{\omega}(\boldsymbol{F}_{ext}, t), \tag{23}$$

thus again stability is ensured. The multiplication of $\boldsymbol{\rho}(\psi)$ is understood component-wise and the passivity analysis for the system with energy tank as outlined in Section III-E can be carried out in a similar manner.

G. Task-energy Based Tank Initialization

Although stability is proven and contact-loss stabilization is ensured, this does not necessarily mean that the task can be fulfilled as desired. If the tank is initially not loaded with sufficient energy, the force controller will be deactivated already during task execution. Thus, the intended task goal will not be achieved (at least not with the desired performance), since force regulation cannot be maintained properly. For this problem, we introduce the concept of task energy E_T, which we define as the minimum initial tank energy that is needed to fulfill the desired task (here: accurate contact force tracking). In order to estimate E_T e.g. for a translational force tracking task, we make use of the static equilibrium of forces

$$\boldsymbol{f}_I|_{\boldsymbol{p}=\boldsymbol{p}_w} + \boldsymbol{f}_d(t) = \boldsymbol{f}_W, \tag{24}$$

where $\boldsymbol{f}_I = K_{x,t}(\boldsymbol{p} - \boldsymbol{p}_s)$ and $\boldsymbol{f}_W$ are the forces due to the impedance stiffness and environmental counter force, respectively. $K_{x,t}$ is the translational stiffness matrix, $\boldsymbol{p}$ is the end-effector position, and $\boldsymbol{p}_s$ is the desired end-effector position. For sake of simplicity let us model the counter force $\boldsymbol{f}_W$ that is generated by the environment as a linear stiffness (without the consideration of damping) between $\boldsymbol{p}$ (in the steady-state case $\boldsymbol{p} = \boldsymbol{p}_w$) and wall set-point $\boldsymbol{p}_{w,0}$ as $\boldsymbol{f}_W = K_{w,t}(\boldsymbol{p}_w - \boldsymbol{p}_{w,0})$. Here, $\boldsymbol{f}_W$ denotes the force exerted by the wall when being in contact and $K_{w,t}$ is the respective (translational) wall stiffness. Solving for $\boldsymbol{p}_w(t)$ yields the wall position after the force is regulated. The work required to move the wall can be calculated as[7]

$$E_T(t) = \int_0^t \frac{1}{2}(\boldsymbol{p}_w(\sigma) - \boldsymbol{p}_{w,0})^T K_{w,t}(\boldsymbol{p}_w(\sigma) - \boldsymbol{p}_{w,0}) d\sigma. \tag{25}$$

For the special regulation case $\boldsymbol{f}_d = const.$ we may calculate the task energy as $E_T = \frac{1}{2}(\boldsymbol{p}_w - \boldsymbol{p}_{w,0})^T K_{w,t}(\boldsymbol{p}_w - \boldsymbol{p}_{w,0})$ and initialize the tank energy accordingly.

IV. SIMULATION

The simulation and experimental validation was carried out with the fully torque-controlled KUKA/DLR LWR-III [23]. The simulation framework was implemented in MATLAB Simulink® and the controllers are designed according to Section III-E. The initial configuration for the simulation of the robot is $\boldsymbol{q}_0 = (0, 0, 0, -90, 0, 90, 0)^T$ [°]. The environment model is a simple virtual wall as described in Section III-G. For the simulation, the wall is located at $\boldsymbol{p}_{w,0} = (0, 0, 0.65)^T$ [m] with a translational stiffness of $K_{w,t} = diag\{250, 250, 250\}$ [N/m]. The end-effector starting position (translation) is $\boldsymbol{p}_0 = (-0.39, 0, 0.71)^T$ [m] and the impedance set-point is located at $\boldsymbol{p}_s = (-0.39, 0, 0.5)^T$ [m]. The remaining parameters and gains can be found in Table I. D_x is designed such that critical damping is achieved as mentioned in Section III-A. Figure 7(a) shows that the force error $f_z = f_{ext,z} - f_{d,z}$ is regulated to zero over time. It also depicts that the tank is filled due to the movement of the robot. Then energy is drained as the integral part draws energy from the tank. In Figure 7(b) the lower tank limit is defined as $T_l = 1$ [J]. The energy is now insufficient and the desired force can not be regulated. We may now calculate the required task energy for our simulation according to Section III-G for $\boldsymbol{f}_d = (0, 0, 5)^T = const.$ as $E_T = \frac{1}{2}(\boldsymbol{p}_w - \boldsymbol{p}_{w,0})^T K_{w,t}(\boldsymbol{p}_w - \boldsymbol{p}_{w,0})$ and initialize the tank with this amount, see Figure 7(c). The force can now be regulated to zero again.

[7]Here we consider only the translational energy.

(a) Initial configuration (phase 1)

(b) Non-contact situation (phase 1)

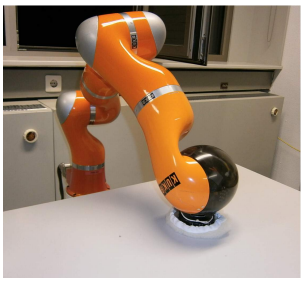

(c) Contact situation and force application (phase 2,3,4a + 4b)

(d) Contact loss (phase 4c)

Fig. 8. KUKA/DLR LWR-III in different phases during the experiments.

V. EXPERIMENTS

For the following two experiments we use a KUKA/DLR LWR-III which initial position is $\boldsymbol{q}_0 = (0, 30, 0, -60, 0, 90, 0)^T$ [°], see Figure 8(a). An aluminum plate is mounted on the end-effector that is covered by wool. Since the robot is not equipped with a force sensor, the external force $\boldsymbol{F}_{ext}$ is obtained via an accurate observer-based estimate [16] and low-pass filtered with a cut-off frequency of 10 [Hz]. Again, D_x is obtained as described in Section IV and all parameters for the experiments are found in Table I. It should be noted that the damping gain in the experiments is set to zero, because otherwise the system becomes unstable. This is due to the fact that no force-torque sensor was used and instead an observer for the external forces whose dynamics is not considered in the tank design.

A. Polishing Task

In the first experiment, the task is to polish a table with a constantly regulated normal force. The robot starts from $\boldsymbol{q}_0$ and is moved via Cartesian impedance control to the vicinity of the table without touching it (phase 1, Figure 8(b)). Afterwards, a contact with the table is established via impedance control (phase 2, Figure 8(c)). Now, the force

TABLE I

GAINS AND PARAMETERS USED IN SIMULATION AND EXPERIMENT.

	$f_{d,z}$ [N]	K_x [N/m, Nm/rad]	K_p	K'_d [s]	K_i [1/s]	T_l [J]	T^u [J]
Simulation	5	diag{1500,1500,1500,200,200,200}	$10I_{6\times6}$	$1I_{6\times6}$	$40I_{6\times6}$	10^{-3}, 1, 4.232	20
Experiments	10	diag{1500,1500,1500,200,200,200}	$1I_{6\times6}$	$0I_{6\times6}$	$2.5I_{6\times6}$	10^{-3}	2000

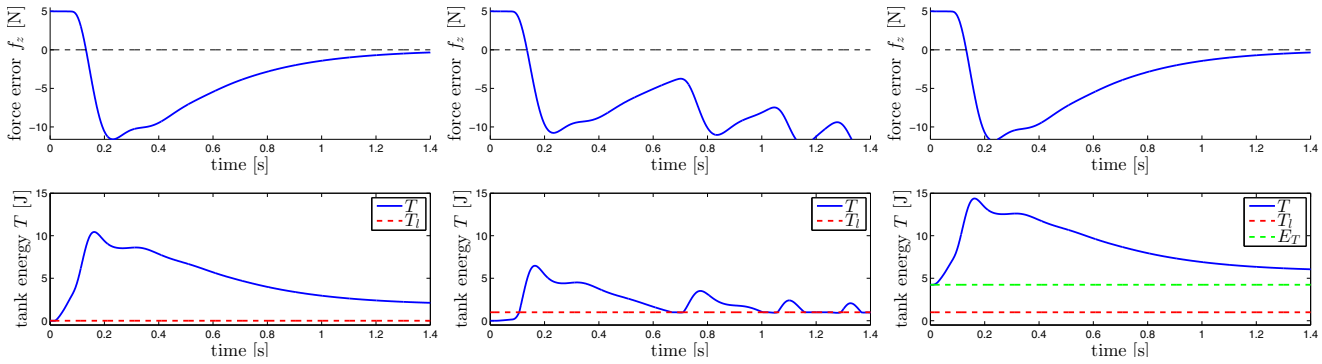

Fig. 7. Simulation results: The upper row depicts the force error $f_z = \hat{f}_{ext,z} - f_{d,z}$ and the lower one shows the tank energy T. Left: The force is accurately regulated to zero. Middle: If the lower bound T_l is chosen too high (here: $T_l = 1$ [J]) then the force cannot be regulated correctly anymore as the task requires too much energy. Right: After calculation of the respective task energy, the tank is initialized with $E_T = 4.232$ [J] and the desired force can be regulated again.

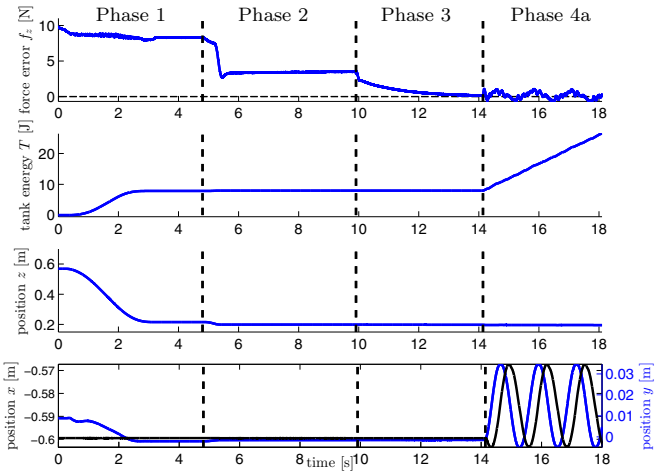

Fig. 9. Polishing task with different phases: Move close to the table (1), establish contact (2), apply force (3), polish the table (4a). Here, the gains are chosen purposely lower to better visualize the force regulation.

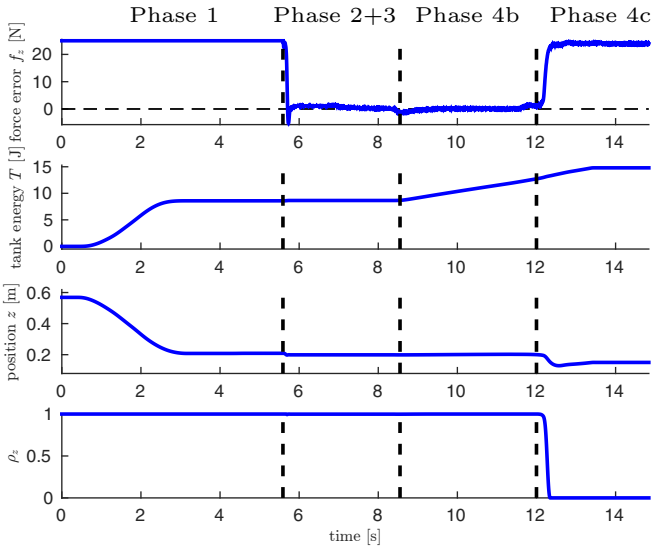

Fig. 10. Handling loss of contact: Move near the table (phase 1), establish contact and apply force (phase 2+3), move in x-direction (phase 4b), move beyond edge of table (phase 4c).

controller is activated together with the impedance controller in order to apply the specified desired force (phase 3). Finally, perpendicular circular motions in the table plane are commanded via a velocity interface to the set-point of the impedance controller (phase 4a). Figure 9 shows the force error in z-direction, the tank energy, z-position, as well as the x- and y-position of the end-effector. The tank is mainly loaded during phase 1 and 4a due to (larger) movements of the end-effector In phase 3 it is only marginally drained by the force controller. This is mainly due to lower gains in comparison to the simulation. It can be seen that by using an impedance controller only (phase 2), there is still a discrepancy in the force error. In phase 3, when the force controller is activated, the force error is regulated to zero. In phase 4a during the tangential (x, y)-polishing task, the force error is around zero. Only very small motion artifacts (e.g. due to friction) remain.

B. Loosing Contact

In order to show how unexpected contact loss, as described in Section III-F, is handled, we show an experiment where the end-effector is placed on the table and is sought to

TABLE II

CONTROLLER COMPARISON.

Properties	Imp. Ctr.	Force Ctr.	Force/Imp. Ctr.
Compliance	✓	✗	✓
Force regulation	✗	✓	✓*
Unmodeled environments	✓	✗	✓
Stability in non-contact	✓	✗	✓
Stability in transition	✓	✗	✓
Stability in contact	✓	✓	✓

apply a desired force. While applying this specified force, a constant velocity is commanded in x-direction inducing a movement towards the edge of the table. Figure 10 shows, similar to the previous example, different phases. Phases 1-3 are identical to the previous experiment. In phase 4b the end-effector moves at constant velocity in x-direction towards the table edge and looses contact in the transition to phase 4c (see Figure 8(d)). It can be seen by observing the z-position that although contact is lost unexpectedly, the end-effector is still nearby the table height and does not move any further towards the ground.

VI. CONCLUSION

In this paper we proposed a novel Cartesian passivity-based force/impedance controller. In order to be able to systematically fuse both concepts, we applied the concept of energy tanks such that the force tracking controller, impedance controller, energy tank, and motor dynamics together yield a passive system. Furthermore, our approach is able to cope with contact discontinuities such that no unwanted rapid motions due to contact loss may occur. To validate our theoretical results, several simulations and experiments were carried out. Conclusively, Table II summarizes the main features of the presented controller and compares it to existing approaches. As already mentioned, if stability needs to be ensured at all times, exact force regulation may not be achieved (*).

In order to get rid of this problem, which is equivalent to the question of how to initialize the energy tank prior to task execution, we introduced the concept of task energy. This is defined as the required energy a force tracking task consumes. By estimating its amount and starting the task after the tank has reached the respective task energy level, we were able to get rid of this known limitation of energy tanks.

REFERENCES

[1] N. Hogan, "Impedance control: An approach to manipulation: Part I - theory, part II - implementation, part III - applications," *ASME Journal of Dynamic Systems, Measurement, and Control*, vol. 107, pp. 1–24, 1985.

[2] A. Albu-Schaffer, M. Fischer, G. Schreiber, F. Schoeppe, and G. Hirzinger, "Soft robotics: what cartesian stiffness can obtain with passively compliant, uncoupled joints?" in *Intelligent Robots and Systems, 2004.(IROS 2004). Proceedings. 2004 IEEE/RSJ International Conference on*, vol. 4. IEEE, 2004, pp. 3295–3301.

[3] L. Villani and J. D. Schutter, "Force control," in *Springer Handbook of Robotics*. Springer, 2008, pp. 161–185.

[4] E. Lutscher and G. Cheng, "Constrained manipulation in unstructured environment utilizing hierarchical task specification for indirect force controlled robots," in *IEEE International Conference on Robotics and Automation 2014 (ICRA2014)*, 2014.

[5] D. Lee and K. Huang, "Passive-set-position-modulation framework for interactive robotic systems," *Robotics, IEEE Transactions on*, vol. 26, no. 2, pp. 354–369, 2010.

[6] G. Borghesan and J. De Schutter, "Constraint-based specification of hybrid position-impedance-force tasks," in *IEEE International Conference on Robotics and Automation 2014 (ICRA2014)*, 2014.

[7] M. Raibert and J. Craig, "Hybrid position/force control of manipulators," *ASME Journal of Dynamical Systems, Measurement and Control*, vol. 105, pp. 126–133, 1981.

[8] G. Zeng and A. Hemami, "An overview of robot force control," *Robotica*, vol. 15, no. 05, pp. 473–482, 1997.

[9] J. Duffy, "The fallacy of modern hybrid control theory that is based on "orthogonal complements" of twist and wrench spaces," *Journal of Robotic Systems*, vol. 7, no. 2, pp. 139–144, 1990.

[10] V. Duindam and S. Stramigioli, "Port-based asymptotic curve tracking for mechanical systems," *European Journal of Control*, vol. 10, no. 5, pp. 411–420, 2004.

[11] J. Cervera, A. Van Der Schaft, and A. Baños, "Interconnection of port-hamiltonian systems and composition of dirac structures," *Automatica*, vol. 43, no. 2, pp. 212–225, 2007.

[12] M. Spong, "Modeling and control of elastic joint robots," *ASME J. on Dynamic Systems, Measurement, and Control*, vol. 109, pp. 310–319, 1987.

[13] A. Albu-Schäffer, C. Ott, and G. Hirzinger, "A unified passivity-based control framework for position, torque and impedance control of flexible joint robots," *The Int. J. of Robotics Research*, vol. 26, pp. 23–39, 2007.

[14] A. Albu-Schäffer, C. Ott, U. Frese, and G. Hirzinger, "Cartesian impedance control of redundant robots: Recent results with the DLR-light-weight-arms," in *Robotics and Automation, 2003. Proceedings. ICRA'03. IEEE International Conference on*, vol. 3. IEEE, 2003, pp. 3704–3709.

[15] C. Ott, A. Albu-Schäffer, A. Kugi, S. Stramigioli, and G. Hirzinger, "A Passivity Based Cartesian Impedance Controller for Flexible Joint Robots - Part I: Torque Feedback and Gravity Compensation," in *IEEE International Conference on Robotics and Automation 2004 (ICRA2004)*, 2004, pp. 2666–2672.

[16] S. Haddadin, *Towards Safe Robots: Approaching Asimov's 1st Law*. Springer Publishing Company, Incorporated, 2013.

[17] H. K. Khalil, "Nonlinear systems, 3rd," *New Jewsey, Prentice Hall*, vol. 9, 2002.

[18] M. Franken, S. Stramigioli, S. Misra, C. Secchi, and A. Macchelli, "Bilateral telemanipulation with time delays: A two-layer approach combining passivity and transparency," *Robotics, IEEE Transactions on*, vol. 27, no. 4, pp. 741–756, 2011.

[19] A. Franchi, C. Secchi, H. I. Son, H. H. Bulthoff, and P. R. Giordano, "Bilateral teleoperation of groups of mobile robots with time-varying topology," *Robotics, IEEE Transactions on*, vol. 28, no. 5, pp. 1019–1033, 2012.

[20] C. Secchi, A. Franchi, H. Bulthoff, and P. R. Giordano, "Bilateral teleoperation of a group of UAVs with communication delays and switching topology," in *Robotics and Automation (ICRA), 2012 IEEE International Conference on*. IEEE, 2012, pp. 4307–4314.

[21] F. Ferraguti, C. Secchi, and C. Fantuzzi, "A tank-based approach to impedance control with variable stiffness." in *IEEE International Conference on Robotics and Automation 2013 (ICRA2013)*, 2013, pp. 4948–4953.

[22] T. S. Tadele, T. J. de Vries, and S. Stramigioli, "Combining energy and power based safety metrics in controller design for domestic robots," in *Robotics and Automation (ICRA), 2014 IEEE International Conference on*. IEEE, 2014, pp. 1209–1214.

[23] G. Hirzinger, N. Sporer, A. Albu-Schäffer, M. Hahnle, R. Krenn, A. Pascucci, and M. Schedl, "DLR's torque-controlled light weight robot III-are we reaching the technological limits now?" in *Robotics and Automation, 2002. Proceedings. ICRA'02. IEEE International Conference on*, vol. 2. IEEE, 2002, pp. 1710–1716.